(Received 28 September 2024, Accepted 23 October 2024, Scheduled 4 November 2024)

Leakage Optimization of Active Magnetically Shielded Isotropic Coils for Electric Vehicle Wireless Charging Systems

Yonghong Long[1], Hui Li[2], Zhongqi Li[1,3*], Bin Li[2], and Ziyue Gan[2]

[1] College of Railway Transportation, Hunan University of Technology, Zhuzhou 412007, China
[2] College of Electrical and Information Engineering, Hunan University of Technology, Zhuzhou 412007, China
[3] College of Electrical and Information Engineering, Hunan University, Changsha 412008, China

ABSTRACT: In the field of wireless power transmission (WPT) for electric vehicles, the challenge of magnetic shielding technology is particularly prominent. Achieving effective magnetic shielding often comes at the cost of transmission efficiency, creating a significant technical bottleneck. As a result, research into improving transmission efficiency while minimizing magnetic leakage has become a primary focus in the industry. This is seen as critical for driving the sustainable development of the electric vehicle sector. In response to this challenge, this paper presents the construction of an active magnetic shield using an isotropic coil configuration, which not only optimizes system efficiency but also significantly reduces magnetic leakage in WPT systems. The paper begins by introducing the concept of an active magnetically shielded isotropic coil structure for wireless power transmission. Next, it details the design methodology and operational principles of the structure, followed by the derivation of the mathematical model and equivalent circuit. The effectiveness of the magnetic shielding mechanism is examined from a theoretical standpoint, and the influence of coil parameters on both shielding performance and transmission efficiency is analyzed. Finally, based on the optimized coil parameters, the design of the wireless charging system incorporating the magnetic shielding structure is completed. This includes relevant theoretical calculations, simulation analyses, and experimental validation to confirm the feasibility of the design. The results demonstrate that the active magnetically shielded isotropic coil significantly reduces magnetic leakage, lowering it by approximately 95.68% compared to traditional coils, while achieving a transmission efficiency of 95.68% in experiments.

1. INTRODUCTION

China's new energy vehicle industry has entered a phase of rapid growth and development [1–3]. According to data released by China's automotive industry authorities, the country has emerged as a global leader in both the production and sales of new energy vehicles [4]. Before the rise of Wireless Power Transfer (WPT), charging stations were the core component of China's electric vehicle charging system. Wireless charging technology presents new opportunities for the automatic charging of electric vehicles, playing a crucial role in achieving fully autonomous driving throughout the entire vehicle lifecycle [5], and currently, China's technology companies and research institutes such as Huawei, ZTE New Energy, and Zhonghui Chuangzhi are actively involved in the field of wireless charging for electric vehicles. In addition, several mainstream automakers are also developing wireless charging systems for electric vehicles [6]. However, as the power increases, wireless charging systems generate high-frequency magnetic fields in the surrounding space during the charging process, posing potential risks to human health [7] and causing interference with the surrounding ecological environment and electronic equipment. This makes the study of electromagnetic shielding technology for wireless charging systems in new energy vehicles particularly necessary and crucial.

In the field of electromagnetic shielding for wireless charging systems in new energy vehicles, the primary methods currently employed include both passive [8] and active shielding [9] strategies. In the passive shielding approach, the choice of shielding materials is particularly crucial, typically falling into two categories: metallic materials [10] and magnetic materials [11]. The shielding principle of metallic materials involves generating a high-frequency interference field within the shield, which induces eddy-current losses and creates reflections at the interface between the shield and protected area, thereby effectively attenuating the electromagnetic field. The core principle behind magnetic materials' shielding lies in their high permeability. This property allows magnetic flux to be effectively confined within the material, increasing the mutual inductance between coils and enhancing the coupling coefficient, while also optimizing the distribution of the magnetic field. Compared to incorporating magnetic materials into the WPT system, the use of metal shielding materials is the primary approach for reducing magnetic leakage. Metal shielding is highly effective in suppressing magnetic field leakage, with fully enclosed conductive shells providing even better shielding. However, the presence of eddy current effects can impact the overall system performance. In 2018, Cruciani's team at the University of L'Aquila in Italy used COMSOL [12] performed a finite element simulation analysis of a WPT system equipped with aluminum plate shielding. The results showed that the magnetic

* Corresponding author: Zhongqi Li (my3eee@126.com).

field strengths on both sides of the car met international standards, regardless of coil alignment or offset. However, since the team designed coils with a small radius of only 25 cm, their conclusions are mainly applicable to small-sized transmission coils. For high-power coils with a radius greater than 25 cm, the safety of electromagnetic radiation still requires further validation. Magnetic material shielding can significantly increase the mutual inductance coefficient, but its shielding effect is limited and prone to magnetic saturation. Active shielding is achieved by applying additional excitation or inverting the shielding coil in series above the main coil to generate a reverse canceling magnetic field [13, 14]. Notably, Cruciani and his team at the University of L'Aquila, Italy, proposed a novel active shielding technique, which involves placing a shielding coil in series with the transmitting coil on the same horizontal plane [12]. While this structure effectively reduces the magnetic field in localized areas, its overall shielding effect on system-wide magnetic leakage remains limited. Kim and his team at the Korea Advanced Institute of Science and Technology (KAIST) observed in their study [15] that placing shielding coils vertically at a distance from both sides helped minimize the interference with the magnetic circuits of the transmitting and receiving coils. However, the shielding effect of this approach was not satisfactory. To improve it, the shielding coils were positioned closer [16], which enhanced the shielding performance to some extent. However, the relationship between equivalent inductance and the shielding effect was not thoroughly modeled or analyzed.

Currently, although extensive research on magnetic shielding methods has been conducted, the challenge of balancing shielding effectiveness with transmission efficiency remains an unsolved issue.

In this paper, an active magnetically shielded isotropic coil structure is proposed to reduce magnetic leakage in WPT system. The transmitter and receiver share the same coil structure, where the main coil consists of two identical coils connected in series in a forward direction. The shielding coil generates opposing magnetic flux by being connected in series in the reverse direction to the main coil, significantly reducing magnetic leakage in the WPT system while maintaining high energy transfer efficiency. The magnetic shielding principle of the proposed coil structure is analyzed in detail, and a coil optimization method is presented to ensure both high transmission efficiency and minimal magnetic leakage. Finally, an experimental platform is successfully constructed, and the reliability of this method is verified.

2. ACTIVE COAXIAL MAGNETIC SHIELDING STRUCTURE AND MAGNETIC SHIELDING PRINCIPLE

In the field of magnetic shielding research, there is often a trade-off between transmission efficiency and shielding effectiveness. The current challenge is how to optimize transmission efficiency while maintaining effective magnetic shielding. Overcoming this technical hurdle is essential for the advancement of wireless energy transmission systems. To address this issue, both unshielded and passive magnetically shielded coaxial coil structures have been introduced as improvements over traditional coils. While these designs provide some level of magnetic shielding, their effectiveness is still limited. As a result, a novel and simplified active magnetically shielded coaxial coil structure has been developed. This new structure is further analyzed using its equivalent circuit model, representing a continued enhancement of previous designs. From a mathematical perspective, the limitations of conventional coil structures, unshielded coaxial coil structures, and passive magnetically shielded coaxial coil structures — namely their inability to balance transmission efficiency and shielding effectiveness — are experimentally demonstrated. The results indicate that the proposed active magnetically shielded coaxial coil structure overcomes these shortcomings, ensuring both high transmission efficiency and reduced magnetic leakage.

2.1. Active Magnetically Shielded Isotropic Coil Structure

The active magnetically shielded isotropic coil structure at the transmitting end consists of two main coils, T_{x1} and T_{x2}, connected in series in the forward direction, along with a shielding coil, T_{Sh}, connected in series in the reverse direction. The receiving end is configured similarly, with coils R_{x1}, R_{x2}, and R_{Sh} arranged in the same manner as the transmitting end. As shown in Figure 1, the transmitting and receiving coils are aligned along the same axis, with a transmission distance of 15 cm between them. The current I direction in T_{Sh} and R_{Sh} is opposite to that in T_{x1}, T_{x2} and R_{x1}, R_{x2}. However, the current direction within T_{x1} and T_{x2}, as well as within R_{x1} and R_{x2}, remains the same.

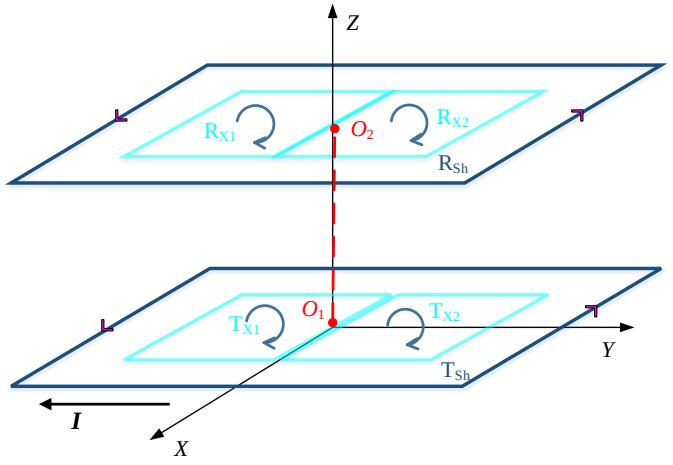

FIGURE 1. Magnetic shielding structure diagram.

Based on the coil structure shown in Figure 1, the corresponding equivalent circuit model can be developed, as illustrated in Figure 2.

In the circuit diagram shown in Figure 2, L_1 and L_2 represent the self-inductance of the transmitting and receiving coils, respectively, while R_1 and R_2 denote their corresponding internal resistances. The resonant capacitances at the transmitter and receiver are denoted by C_{Tx} and C_{Rx}, respectively. M_{12} represents the mutual inductance between the two, and R_s denotes the internal resistance of the power supply V_s at the transmitter. Based on these parameters, the following matrix of Kirchhoff

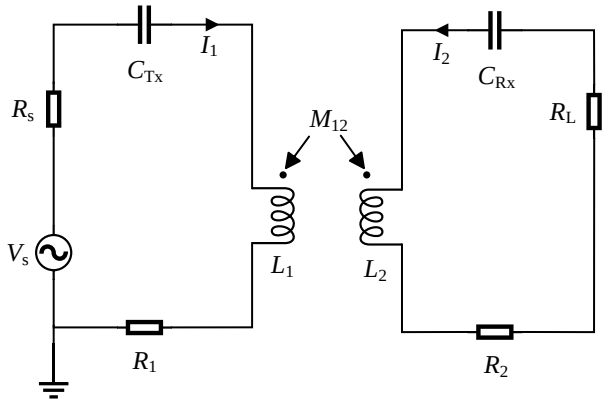

FIGURE 2. Equivalent circuit model of two coils.

voltage equations can be derived:

$$\begin{bmatrix} Z_1 & j\omega M_{12} \\ j\omega M_{12} & Z_2 \end{bmatrix} \begin{bmatrix} I_1 \\ I_2 \end{bmatrix} = \begin{bmatrix} V_s \\ 0 \end{bmatrix} \tag{1}$$

Equation (2) represents the currents in the transmitting and receiving coils, respectively.

$$\begin{cases} I_1 = \frac{Z_2 V_S}{Z_1 Z_2 + (\omega M_{12})^2} \\ I_2 = -\frac{j\omega M_{12} V_S}{Z_1 Z_2 + (\omega M_{12})^2} \end{cases} \tag{2}$$

Z_1 represents the impedance of the coil at the transmitter end, while Z_2 refers to the impedance of the coil at the receiver end.

$$\begin{cases} Z_1 = R_S + R_1 + j\omega L_1 - j\frac{1}{\omega C_{Tx}} \\ Z_2 = R_2 + R_L + j\omega L_2 - j\frac{1}{\omega C_{Rx}} \end{cases} \tag{3}$$

From Equation (4), the system transmission efficiency, denoted as η, can be determined.

$$\eta = \left| \frac{I_2^2 R_L}{V_S I_1} \right| = \left| -\frac{(\omega M_{12})^2 R_L}{Z_1 Z_2^2 + (\omega M_{12})^2 Z_2} \right| \tag{4}$$

At system resonance, $Z_1 = R_1 + R_s$, $Z_2 = R_2 + R_L$, from which the updated expression for transmission efficiency is derived:

$$\eta = \frac{(\omega M_{12})^2 R_L}{(R_S + R_1)(R_2 + R_L)^2 + (\omega M_{12})^2 (R_2 + R_L)} \tag{5}$$

At the maximum transmission efficiency, the optimal load R_{Lopt} can be calculated using the following expression:

$$R_{\text{Lopt}} = \sqrt{\frac{(R_S + R_1) R_2^2 + (\omega M_{12})^2 R_2}{(R_S + R_1)}} \tag{6}$$

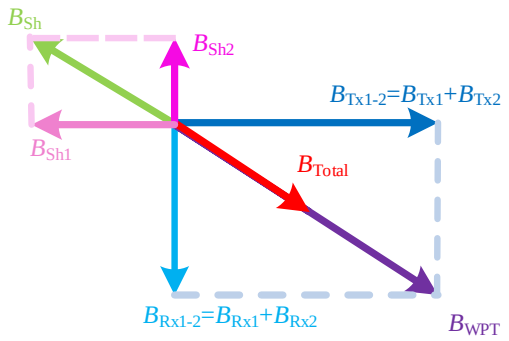

FIGURE 3. Magnetic field vector superposition schematic.

2.2. Principle of Magnetic Shielding

To more intuitively illustrate the magnetic field weakening effect of this structure, it can be demonstrated using the magnetic field vector superposition diagram, as shown in Figure 3.

Here, B_{Tx1} and B_{Tx2} represent the magnetic field vectors of the transmitting coils T_{x1} and T_{x2}, respectively. Since T_{x1} and T_{x2} are connected in series in the same direction, their magnetic field vectors align. The resulting combined magnetic field vector is denoted as B_{Tx1-2}, where B_{Tx1-2}=B_{Tx1} + B_{Tx2}. The T_{Sh} coil is connected in reverse series with T_{Tx1-2}, causing the magnetic field vector B_{Sh1} of T_{Sh} to oppose B_{Tx1-2}. The receiving coils are configured similarly to the transmitting coils, with R_{Sh} and R_{x1-2} connected in reverse series, producing magnetic field vectors B_{Sh2} that opposes B_{Rx1-2}. As a result, the magnetic field formed by the shielding coil is canceled with the magnetic field B_{WPT} (consisting of B_{Tx1-2} − B_{Rx1-2}) in the wireless energy transmission system. By adjusting the parameters of the shielding coil, it helps to significantly reduce the overall magnetic field B_{Total}.

In this section, the magnetic flux density is derived using the method for calculating the magnetic field of a rectangular coil, as outlined in [18]:

$$\mathbf{B}_X = \frac{1}{4\pi^2} \int_{-\infty}^{\infty} \int_{-\infty}^{\infty} \frac{j2\mu_0 I \sin(\xi a_1) \sin(\eta a_2)}{\eta} e^{j(x\xi + y\eta)} d\xi d\eta \tag{7}$$

$$\mathbf{B}_Y = \frac{1}{4\pi^2} \int_{-\infty}^{\infty} \int_{-\infty}^{\infty} \frac{j2\mu_0 I \sin(\xi a_2) \sin(\eta a_1)}{\xi} e^{j(x\xi + y\eta)} d\xi d\eta \tag{8}$$

$$\mathbf{B}_Z = \frac{1}{4\pi^2} \int_{-\infty}^{\infty} \int_{-\infty}^{\infty} \frac{-2\mu_0 I q \sin(\xi a_1) \sin(\eta a_2)}{\xi\eta} e^{j(x\xi + y\eta)} d\xi d\eta \tag{9}$$

$$B = \sqrt{B_X^2 + {B_Y}^2 + {B_Z}^2} \tag{10}$$

Here, ξ and η are the variables of the double Fourier integral; a_1 and a_2 represent the half-length and half-width of the coil at the transmitter end; I denotes the current flowing through the transmitter coil, $q = \sqrt{\xi^2 + \eta^2}$.

The mutual inductance between multi-turn coils can be calculated from (11):

$$M = \sum_{m=1}^{N_1} \sum_{n=1}^{N_2} M_{mn} \tag{11}$$

where N_1 represents the number of turns in the transmitting coil, N_2 the number of turns in the receiving coil, m the m-th turn of the transmitting coil, and n the n-th turn of the receiving coil.

3. DESIGN OF A NEW ACTIVE ISOTROPIC SHIELDED COIL

This section provides a detailed description of the design scheme for the entire shielding system, including the design of the source and shielding coils, as well as the selection of shielding coil parameters. Additionally, the distance between the shielding coil and main coil is discussed to ensure the safety of the overall system. Finally, the system parameters are determined to facilitate experimental validation.

3.1. Optimization of Magnetic Leakage

The active magnetically shielded isotropic coil structure presented in this paper is designed to reduce magnetic field leakage in the horizontal direction. In vehicle applications, the coils are typically placed in parking spaces and at the center of the vehicle chassis. The magnetic field leakage is measured at an observation point approximately 80 cm horizontally from the vehicle's center and perpendicular to the ground. To ensure system safety, the magnetic field leakage at 80 cm and beyond must remain within safe limits. Therefore, during system operation, it is crucial to monitor the magnetic field distribution at the 80 cm horizontal plane to accurately identify any new maximum leakage points and ensure that the system operates stably within safety standards. The coil optimization flowchart is shown in Figure 4.

In this section, the coil parameters of the magnetic shielding system are optimized using the formula for calculating the magnetic field of a rectangular coil. The goal is to ensure that the magnetic leakage at the system's maximum leakage point remains within safe limits at an output power of 4 kW. The optimization steps are as follows:

(1) Parameter Setting and Initialization: The vertical distance between the transmitting and receiving coils is set to 15 cm. The wire is copper with a cross-sectional diameter of 0.39 cm. The maximum magnetic induction strength is limited to 27 μT, the output power is fixed at 4 kW, and the transmission efficiency is set to 95%.

(2) Setting Constraints: The parameters are defined based on actual conditions. The dimensional parameters of the receiving and transmitting coils are kept the same. The inner edge lengths of T_{x1} and T_{x2} are set between 25 and 35 cm, and the number of turns is set between 18 and 25. The distances of the shielding coil T_{Sh} from the main coils T_{x1} and T_{x2} are set between 5 and 10 cm, with the number of turns ranging from 3 to 8. The step size for the number of turns is 1 turn, and the step size for both the inner edge length and distance is set to 1 cm.

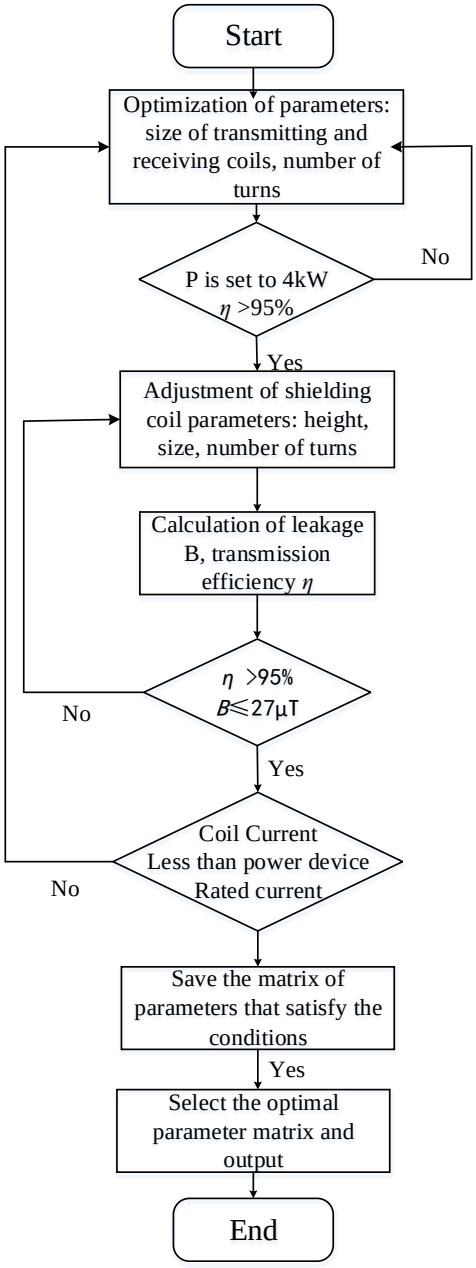

FIGURE 4. Optimization flowchart.

(3) Calculation of Magnetic Leakage B: The maximum leakage at the critical point is calculated using Equation (10), with the receiving coil offset in 2 cm increments, up to a total offset of 10 cm. The maximum leakage point is identified on the observation plane, defined by an X-axis range of $(-100, 100)$ cm, a Z-axis range of $(0, 70)$ cm, and a Y-axis value of 80 cm.

(4) Conditions: The magnetic leakage B must be less than 27 μT to ensure the safety of the magnetic field, and the transmission efficiency must reach 95% to maintain efficient system operation. Only when both conditions are satisfied can the system proceed to the next step. If these conditions are not met, the coil parameters are adjusted, and the optimization process continues until all parameters have been evaluated.

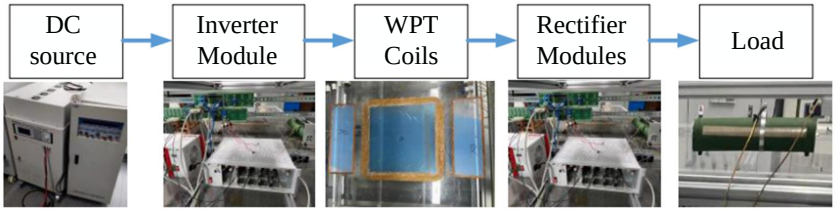

FIGURE 5. System experimental framework diagram.

(5) Output of Optimal Matrix Parameters: The magnetic leakage B on the observation surface is minimized while ensuring a transmission efficiency $\eta > 95\%$.

3.2. Optimization Results

By applying the parameter optimization strategy outlined in the previous subsection, the optimal coil parameters that meet the system requirements are selected. Table 1 provides the detailed number of turns and sizes for each coil in the system.

TABLE 1. Size and number of turns of each coil.

Coil	Inner length/cm	Inner width/cm	Outer length/cm	Outer width/cm	Number of turns
T_{x1}	30.0	30.0	45.2	45.2	20
T_{x2}	30.0	300	45.2	45.2	20
T_{Sh}	107.6	61.2	110.8	64.8	5
R_{x1}	30.0	30.0	45.2	45.2	20
R_{x2}	30.0	30.0	45.2	45.2	20
R_{Sh}	107.6	61.2	110.8	64.8	5

4. EXPERIMENTAL VERIFICATION

To verify the effectiveness of the proposed structure and its safety for the human body, this section presents experimental validation. The magnetic leakage B at the system's maximum leakage point on the observation surface and the transmission efficiency η are obtained through three methods: theoretical calculations, Ansys Maxwell electromagnetic simulation data, and physical experimental measurements.

4.1. Experimental Setup

Some of the experimental equipment used in the experiment, along with the framework of the experimental system, is shown in Figure 5.

In Figure 5, the DC power source is converted into high-frequency AC by inverter module, which is then supplied to the transmitting coil. Energy is transferred from the transmitting coil to the receiving coil, and finally, the rectifier module converts the AC from the receiving coil back into DC for the load. Both the inverter and rectifier modules are single-phase full-bridge circuits utilizing SiC power devices. The SiC model used is C3M0075120D, with a maximum allowable current of 30 A.

Figure 6 shows the laboratory setup of a 4 kW test platform, which includes: an oscilloscope, a load, a DC power supply, an RT-unit inverter-rectifier module, a WT5000 power analyzer, an NF-5035S electromagnetic radiation analyzer, and a physical model of the coil.

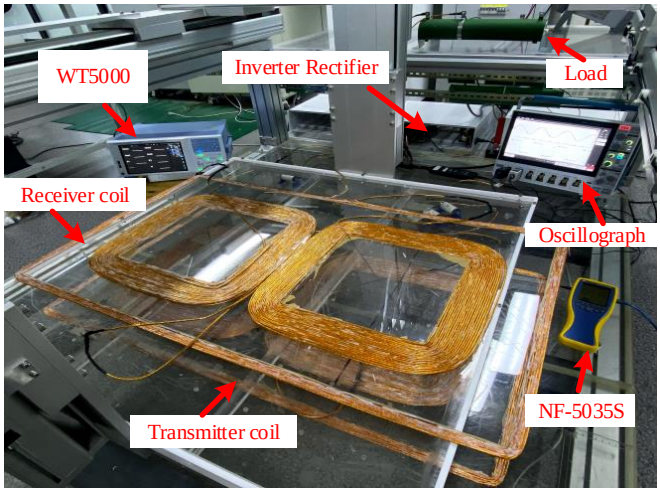

FIGURE 6. Experimental platform.

First, the physical parameters of the coil structure are measured in detail using the IM3536 impedance analyzer to ensure data accuracy. Next, an oscilloscope is used to monitor the voltage and current waveforms of the coil in real time, ensuring that the system reaches resonance. The voltage of the DC power supply is then adjusted, and the system's transmission efficiency is measured using the WT5000 power analyzer. Finally, the NF-5035S electromagnetic radiation analyzer, combined with MCS electromagnetic radiation analysis software, efficiently detects magnetic field changes on the target surface to ensure the system's safety and performance.

Table 2 provides the detailed physical parameters of the experimentally measured active magnetically shielded coaxial coil structure. During the experimental phase, the transmitting and receiving coils (T_x and R_x) had identical structures to enable a comparison of the differential performance of various configurations in terms of magnetic leakage and transmission efficiency. This was done to evaluate the effectiveness of the active magnetically shielded coaxial coils. All coils were wound with 0.1 m $\times$ 800 strands of Litz wire, and the maximum current carrying capacity of the coils was 31.415 A.

TABLE 2. Measurement parameters of coil.

Physical meaning	Parameter	Value
Resonant capacitance of the transmitting coil	C_{Tx}/nF	7.31
Resonant capacitance of the receiving coil	C_{Rx}/nF	7.31
Self-inductance of the transmitting coil	L_1/μH	479.31
Self-inductance of the receiving coil	L_2/μH	479.49
Parasitic resistance of the transmitting coil	R_1/mΩ	290
Parasitic resistance of the receiving coil	R_2/mΩ	280
Operating frequency	f_0/kHz	85
Load	R_L/Ω	33.17

4.2. Leakage Magnetic Field of the System

The effectiveness of active isotropic magnetic shielding structures in reducing magnetic leakage is verified by comparing the maximum magnetic leakage on the target surface across four different structures, all measured at the same offset distance, as shown in Figure 7.

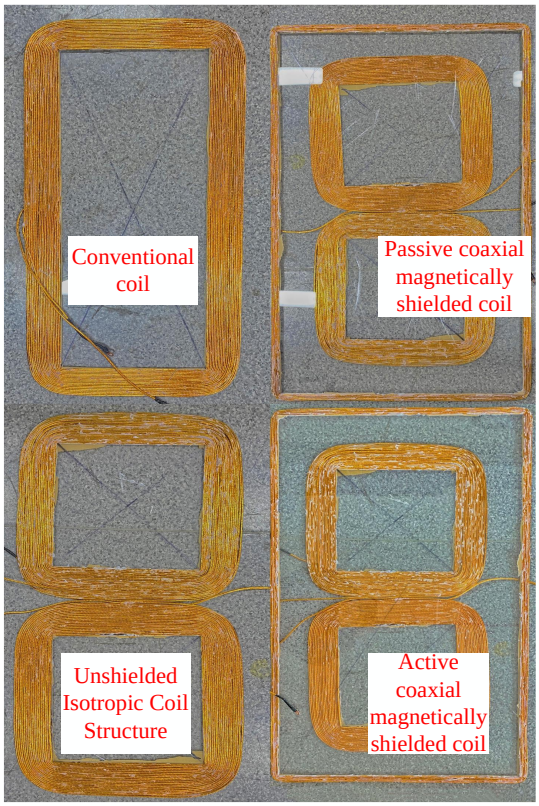

FIGURE 7. Physical diagram of the coil.

For data comparison, Matlab software was first used to accurately calculate the system's leakage magnetic field, yielding the theoretical value B_c. Next, coil models for both the experimental and control groups were constructed and simulated using Ansys Maxwell software, providing the simulation value B_s. Finally, the leakage magnetic field of each structure was measured precisely using an NF-5035S electromagnetic radiation analyzer, resulting in the experimental value B_c.

ε_c is defined as the deviation between the magnetic field value obtained from theoretical calculations and the value obtained from experimental measurements, while ε_s represents the error between the magnetic field values derived from the simulation and experimental measurements. They are computed as follows:

$$\varepsilon_s = \frac{|B_s - B_e|}{B_e} \tag{12}$$

$$\varepsilon_c = \frac{|B_c - B_e|}{B_e} \tag{13}$$

The theoretical, simulated, experimental values, and error rates of the magnetic field when the receiver end of various coil configurations is deflected along the Y-axis are presented in Tables 3, 4, 5, and 6, respectively. Based on the data, none of the error rates exceed 5%, indicating a strong correlation between the theoretical and simulated results.

Table 3 presents the calculated, simulated, and measured values of the magnetic field, along with the corresponding error rates, when the system is offset along the Y-axis by 0–10 cm in the conventional coil structure. Notably, the maximum measured magnetic leakage at an offset distance of 10 cm is 16.699 μT. After comparison, the maximum error between the theoretical and experimental values is controlled to be less than 3.38%, while the maximum error between the simulated and experimental values is 3.26%.

Table 4 presents the theoretical, simulated, and measured values of the magnetic field, along with the corresponding er-

TABLE 3. Theoretical predictions, simulation results, experimental data and error rates of receiving coils with conventional coil structure in Y-axis magnetic field.

Offset distance/cm	B_c/μT	B_s/μT	B_e/μT	ε_s (%)	ε_c (%)
0	14.591	14.614	14.377	1.65	1.49
2	14.803	15.055	15.321	1.74	3.38
4	15.132	15.235	15.506	1.75	2.41
6	15.552	15.562	16.086	3.26	3.32
8	16.097	16.232	16.275	0.26	1.09
10	16.966	16.875	16.699	1.06	1.60

TABLE 4. Theoretical predictions, simulation results, experimental measurements and error rates of the magnetic field in the Y-axis direction of an unshielded receiving coil.

Offset distance/cm	B_c/μT	B_s/μT	B_e/μT	ε_s (%)	ε_c (%)
0	13.432	13.505	13.169	2.55	2.00
2	13.824	13.860	14.277	2.92	3.17
4	14.104	14.134	14.302	1.17	1.38
6	14.610	14.672	14.937	1.77	2.19
8	15.265	15.376	15.073	2.01	1.27
10	16.257	16.481	16.684	1.22	2.56

TABLE 5. Theoretical, simulated, experimental values and magnetic field error rate of the receiving coil along the Y-axis in the case of a passive isotropic magnetic shield structure.

Offset distance /cm	B_c/μT	B_s/μT	B_e/μT	ε_s (%)	ε_c (%)
0	9.515	9.502	9.693	1.97	1.84
2	9.534	9.574	9.611	0.38	0.80
4	10.156	10.169	10.513	3.27	3.40
6	10.585	10.612	10.628	1.08	1.33
8	11.437	11.468	11.633	1.42	1.68
10	12.525	12.568	12.643	0.59	0.93

TABLE 6. Theoretical, simulated, and experimental values and magnetic field error rates of the receiving coil magnetic field of an active isotropic magnetic shield structure at offset along the Y-axis.

Offset distance /cm	B_c/μT	B_s/μT	B_e/μT	ε_s (%)	ε_c (%)
0	5.744	5.736	5.859	2.10	1.96
2	5.754	5.847	5.881	0.58	2.16
4	6.225	6.262	6.077	3.04	2.44
6	6.624	6.815	6.826	0.16	2.96
8	7.475	7.668	7.315	4.83	2.19
10	8.782	8.865	8.694	1.97	1.01

TABLE 7. Theoretical predictions, simulation results, experimental data, and error rates for the transmission efficiency of receiving coils in the Y-axis direction for conventional coil structures.

Offset distance/cm	η_c (%)	η_s (%)	η_e (%)
0	98.81	98.62	96.51
2	98.80	98.61	96.37
4	98.78	98.59	95.23
6	98.76	98.55	95.19
8	98.74	98.53	95.16
10	98.70	98.47	94.37

TABLE 8. Theoretical Predictions, Simulation Results, Experimental Measurements, and Error Rates for Transmission Efficiency of Unshielded Receiving Coils in the Y-axis Direction.

Offset distance/cm	η_c (%)	η_s (%)	ηe (%)
0	98.24	98.02	97.01
2	98.23	98.00	95.11
4	98.20	97.97	94.73
6	98.16	97.93	94.53
8	98.12	97.89	93.82
10	98.00	97.80	93.68

ror rates, when the system is offset along the Y-axis by 0 to 10 cm under the unshielded isotropic coil structure. At an offset distance of 10 cm, the maximum measured magnetic leakage is 16.684 μT, slightly lower than that of the conventional coil structure. However, the effect is not yet significant. The data show that the maximum error between the theoretical and experimental values is 3.17%, while the maximum error between the simulated and experimental values is reduced to 2.92%.

Table 5 presents the calculated, simulated, and measured values of the magnetic field, along with the corresponding error rates, for the passive magnetically shielded isotropic coil structure when the system is offset along the Y-axis from 0 to 10 cm. At the maximum offset of 10 cm, the measured magnetic leakage is 12.643 μT, further reduced compared to the previous two configurations. The maximum error between the theoretical and experimental values is 3.40%, while the maximum error between the simulated and experimental values is only 3.27%.

Table 6 presents the calculated, simulated, and measured magnetic field values, along with the error rates, for the active magnetically shielded isotropic coil structure when the system is offset from 0 to 10 cm along the Y-axis. At a 10 cm offset, the measured maximum leakage field is 8.694 μT, which is 59.25% lower than the maximum leakage field of the conventional coil structure, 55.51% lower than that of the unshielded isotropic structure, and 39.55% lower than the unshielded coaxial magnetically shielded structure. Additionally, the maximum deviation between the theoretical and experimental magnetic field measurements is only 2.96%, while the maximum error between the simulated and experimental measurements is 4.83%. Both errors are controlled within 5%. These results demonstrate that the active isotropic magnetic shielding structure reduces nearly half of the magnetic leakage on the target surface and provides superior shielding performance compared to the other three coil structures of the same size.

Figure 8 illustrates the variation curve of magnetic leakage with offset, based on data from Tables 3 to 6. It is evident that the magnetic leakage of the active isotropic magnetically shielded coil is significantly reduced across all offset conditions. Moreover, the convergence of the calculated, simulated, and measured values confirms the effectiveness of the proposed coil design.

4.3. Transmission Efficiency of the System

To analyze and verify the effectiveness of the active coaxial shielding structure, this study compares its transmission efficiency with that of a conventional coil structure, an unshielded coaxial structure, and a passive coaxial coil structure, all at the same offset distance.

Firstly, the theoretical transmission efficiency, denoted as η_c, can be calculated. Additionally, the simulation value, η_s, is obtained using Matlab/Simulink. Finally, the actual measurement is performed using a WT5000 power analyzer to obtain the experimental value, η_e.

The data in Tables 7 through 10 reveal significant variations in transmission efficiency across different coil configurations,

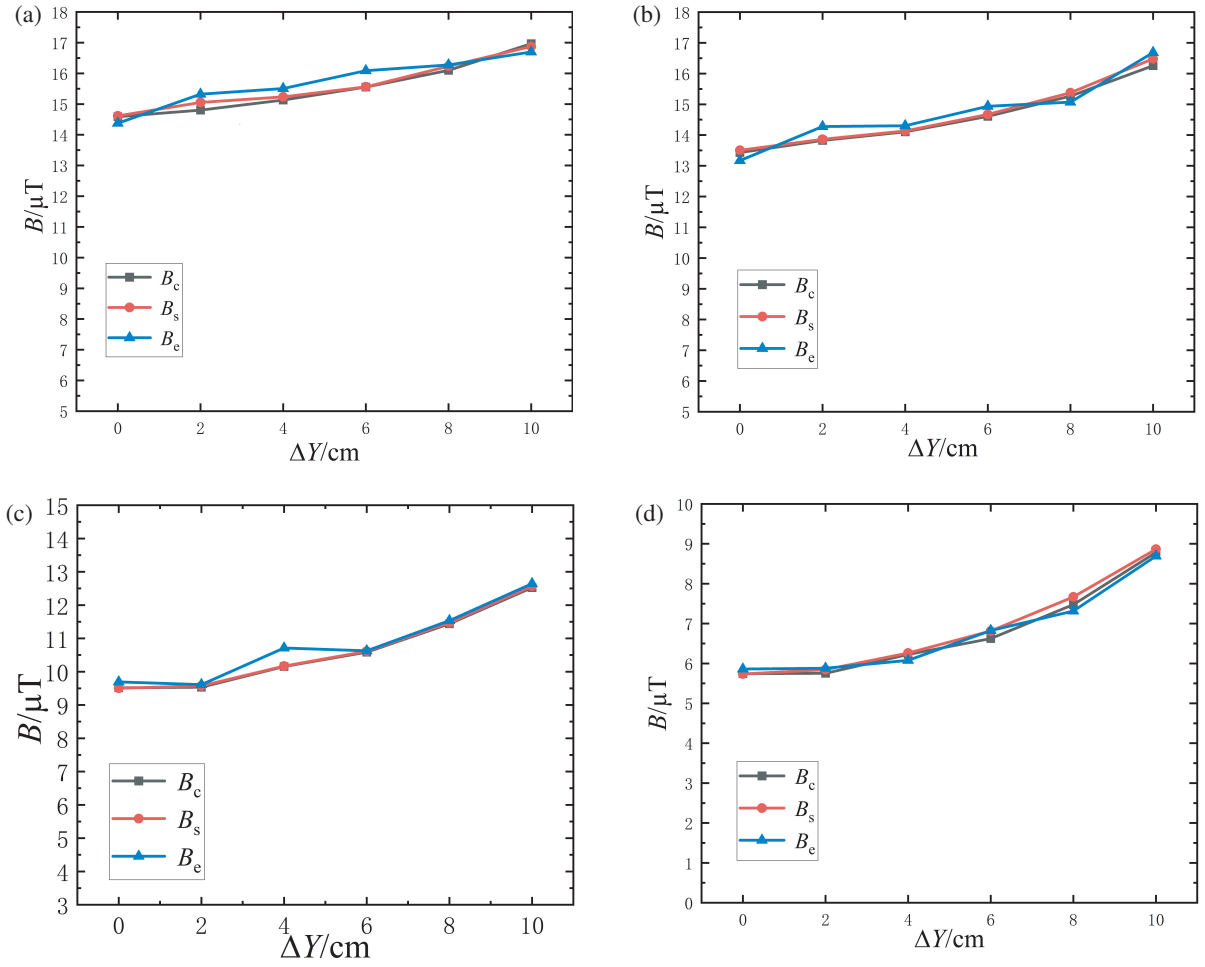

FIGURE 8. Magnetic field leakage with different shielding configurations. (a) Traditional coil structure. (b) Unshielded codirectional coil structure. (c) Passive codirectional magnetic shielding coil structure. (d) Active codirectional magnetic shielding coil structure.

TABLE 9. Theoretical, simulated, experimental values and error rates of receiving coil transmission efficiency along the Y-axis for passive isotropic magnetic shielding structures.

Offset distance/cm	η_c (%)	η_s (%)	η_e (%)
0	97.42	97.22	96.34
2	97.40	97.19	95.04
4	97.36	97.16	94.82
6	97.29	97.03	94.75
8	97.11	96.89	93.71
10	96.80	96.51	93.62

TABLE 10. Theoretical, simulated, and experimental values and error rates of the transmission efficiency of the receiving coil along the Y-axis for active isotropic magnetically shielded structures.

Offset distance/cm	η_c (%)	η_s (%)	η_e (%)
0	96.71	96.45	95.68
2	96.67	96.41	95.33
4	96.54	96.27	95.26
6	96.26	95.98	94.75
8	95.85	95.55	93.68
10	95.18	94.88	93.57

including conventional, unshielded coaxial, passive coaxial, and active coaxial structures. As the offset distance increases, a clear decreasing trend in system efficiency is observed, highlighting the substantial impact of offset distance on overall system performance.

Table 10 demonstrates that the transmission efficiency of the active isotropic structure remains high even when the coil is offset, indicating that this structure maintains efficient performance under offset conditions.

Tables 7 through 10 show that the minimum transmission efficiency observed in real measurements is slightly lower for the active coaxial magnetically shielded coils — 0.8% lower than conventional coils, 0.11% lower than unshielded coaxial coils, and 0.05% lower than passive coaxial magnetically shielded coils. This indicates that, while the active coaxial magnetic shielding results in a slight reduction in transmission efficiency, it significantly improves magnetic shielding, achieving the goal of high-efficiency transmission with reduced magnetic leakage.

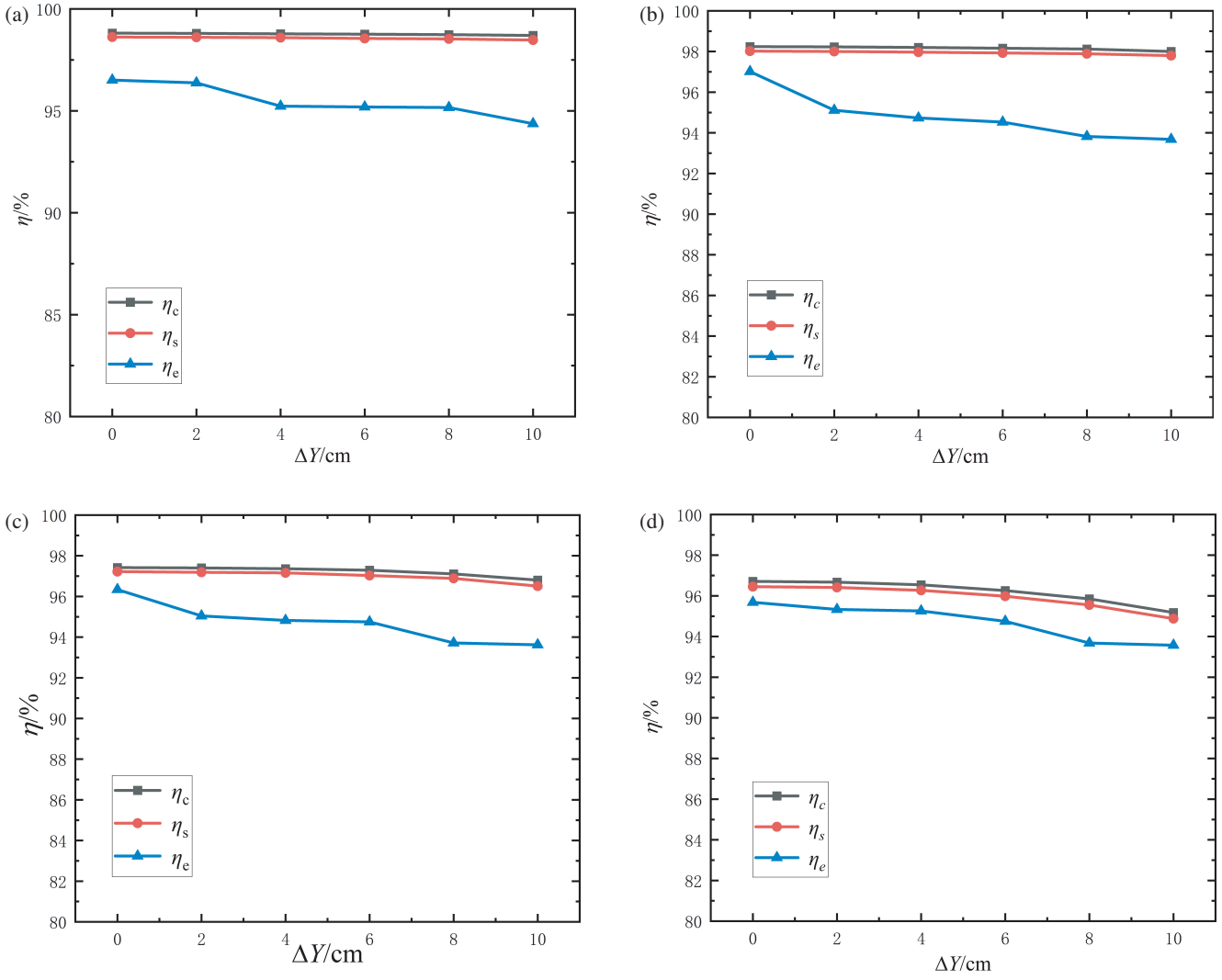

FIGURE 9. Transfer efficiency under different shielding conditions. (a) Traditional coil structure. (b) Unshielded codirectional coil structure. (c) Active codirectional magnetic shielding coil structure. (d) Active codirectional magnetic shielding coil structure.

By analyzing the magnetic leakage and transmission efficiency of different structures, it is evident that the active magnetically shielded isotropic coil structure proposed in this paper maintains high transmission efficiency. While its transmission efficiency is comparable to that of the traditional coil structure, it reduces magnetic leakage by 59.25%, demonstrating a highly effective magnetic shielding performance.

Finally, as shown in Figure 9, the curve illustrating the change in transmission efficiency with offset distance is plotted based on the data from Tables 7 through 10. This visualizes the calculated, simulated, and measured transmission efficiencies, revealing consistent trends across different shielding environments. The active isotropic magnetic shielding coils significantly improve the magnetic shielding effect while only slightly reducing transmission efficiency. This further confirms the high transmission efficiency characteristics of the proposed coil.

5. CONCLUSION

This paper proposes a novel active isotropic magnetic shielding structure that effectively reduces magnetic leakage while maintaining high transmission efficiency, demonstrating excellent safety and reliability. By utilizing the optimal parameter sizes determined through the proposed optimization method, the magnetic leakage at the target surface meets the safety criteria for a magnetic leakage field at a transmission power of 4 kW. Experimental results show that the active isotropic magnetic shielding structure achieves a safe magnetic leakage level of 5.74 μT when the coil is not offset, while maintaining a transmission efficiency of 95.68%. Comparative analysis of theoretical, simulated, and experimental data reveals that, compared to conventional coils, unshielded coaxial coils, and passive coaxial coils, the active isotropic coil structure reduces the maximum measured leakage magnetic field by 59.25%, 55.51%, and 39.55%, respectively, while preserving high efficiency. This demonstrates the structure's ability to synchronize high transmission efficiency with low magnetic leakage.

Even without the use of a ferrite core, the structure effectively reduces the maximum magnetic leakage in the target area to a safe level, significantly lowering the cost of the wireless energy transmission system and enhancing its practical application value. Future research should focus on simplifying this structure to further reduce magnetic leakage above the coil, decrease material costs, and improve transmission efficiency.

ACKNOWLEDGEMENT

This work was supported in part by the National Key R&D Program Project (2022YFB3403200), Hunan Provincial Natural Science Foundation (2022JJ30226), Key Project of Hunan Provincial Department of Education (23A0432), National Natural Science Foundation of China Youth Science Foundation Project: 62303178 Research on High Performance Flexibility and Coordinated Control Methods of Heavy Duty Railway Rail Grinding Robot, Hunan Provincial Department of Education Outstanding Youth Project of Scientific Research Project: 22B0577 Intelligent Decision-making and Cooperative Control of Braking Process of Fast and Heavy Duty Train on Long Downhill Section, and Aid program for Science and Technology Innovative Research Team in Higher Educational Institutions of Hunan Province.

REFERENCES

[1] Li, Z., X. Xiong, P. Kong, and L. Ren, "Research on electromagnetic shielding and efficiency optimization technology of wireless power transfer system," *Journal of Electronic Measurement and Instrumentation*, Vol. 37, No. 5, 151–162, 2023.

[2] Zi, J., D. Qiu, W. Xiao, *et al.*, "Review of key technologies of three-phase wireless charging system for electric vehicles," *Journal of Power Supply*, Vol. 20, 24–33, 2022.

[3] Deng, J. W., "Adaptation and substitution: A governance picture and response strategy for sustainable transformation of urban transportation," *Journal of East China University of Science and Technology (Social Science Edition)*, Vol. 35, 110–124, 2020.

[4] Wu, X. K., Q. X. Yang, X. Zhang, L. H. Zhu, and G. X. Qi, "Coil structure study and efficiency analysis for the driving wireless charging system of electric car," *Advanced Technology of Electrical Engineering and Energy*, Vol. 35, No. 9, 8–13, 2016.

[5] Yang, Q., X. Zhang, and P. Zhang, "Intelligent wireless power transmission cloud network for electric vehicles," *J. Electr. Eng. Technol*, Vol. 38, 1–12, 2023.

[6] Chen, L. S., "Present status and future trends of electric vehicles," *Science and Technology Review*, Vol. 23, 24–28, 2005.

[7] Wu, L. and B. Zhang, "Overview of static wireless charging technology for electric vehicles: Part I," *Transactions of China Electrotechnical Society*, Vol. 35, No. 6, 1153–1165, 2020.

[8] Mohammad, M., M. S. Haque, and S. Choi, "A litz-wire based passive shield design to limit EMF emission from wireless charging system," in *2018 IEEE Energy Conversion Congress and Exposition (ECCE)*, 97–104, Portland, OR, USA, Sep. 2018.

[9] Campi, T., S. Cruciani, F. Maradei, and M. Feliziani, "Magnetic field mitigation by multicoil active shielding in electric vehicles equipped with wireless power charging system," *IEEE Transactions on Electromagnetic Compatibility*, Vol. 62, No. 4, 1398–1405, 2020.

[10] Zhu, Q., D. Chen, L. Wang, C. Liao, and Y. Guo, "Study on the magnetic field and shielding technique for an electric vehicle oriented wireless charging system," *Transactions of China Electrotechnical Society*, Vol. 30, No. S1, 143–147, 2015.

[11] Lee, S.-Y., Y.-S. Lim, I.-H. Choi, D.-I. Lee, and S.-B. Kim, "Effective combination of soft magnetic materials for magnetic shielding," *IEEE Transactions on Magnetics*, Vol. 48, No. 11, 4550–4553, 2012.

[12] Cruciani, S., T. Campi, and M. Feliziani, "Active shielding design for wireless power transfer systems," *IEEE Transactions on Electromagnetic Compatibility*, Vol. 61, No. 6, 1953–1960, 2019.

[13] Meng, J., Y. Zhang, and e. al., "Research of active magnetic shielding for wireless power transfer system of electric vehicles," *Advanced Technology of Electrical Engineering and Energy*, Vol. 40, No. 4, 44–51, 2021.

[14] Li, J., H. Wen, K. Zhang, *et al.*, *Progress of Electromagnetic Interference Suppression in Magnetically Coupled Wireless Energy Transmission Systems*, 7387–7403, 2022.

[15] Kim, S., J. Kim, S. Kong, H. Kim, I.-S. Suh, N. P. Suh, D.-H. Cho, J. Kim, and S. Ahn, "Coil design and shielding methods for a magnetic resonant wireless power transfer system," *Proceedings of the IEEE*, Vol. 101, No. 6, 1332–1342, 2013.

[16] Moon, H., S. Kim, H. H. Park, *et al.*, "Design of a resonant reactive shield with double coils and a phase shifter for wireless charging of electric vehicles," *IEEE Transactions on Magnetics*, Vol. 51, No. 3, 1–4, 2015.

[17] Cruciani, S., T. Campi, M. Feliziani, *et al.*, "Active shielding design for a dynamic wireless power transfer system," in *2020 International Symposium on Electromagnetic Compatibility-EMC EUROPE*, Vol. 51, No. 3, 23–25, Rome, Italy, Sep. 2020.

[18] Li, Z. Q., J. Li, C. H. Quan, X. Y. Zhang, S. D. Huang, *et al.*, "Mutual inductance calculation of arbitrarily positioned rectangular coils with magnetic shielding in wireless power transfer systems," *Transaction of China Electrotechnical Society*, Vol. 37, No. 17, 4294–4305, 2022.